Sensors and Actuators A 277 (2018) 73–84

Contents lists available at ScienceDirect

Sensors and Actuators A: Physical

journal homepage: www.elsevier.com/locate/sna

Design, fabrication and performance evaluation of a printed-circuit-board microfluidic electrolytic pump for lab-on-a-chip devices

Hakhyun Kim, Heewon Hwang, Seonhyeok Baek, Dohyun Kim *

Department of Mechanical Engineering, Myongji University, 116 Myongji-ro, Yongin, 17058, Republic of Korea

ARTICLE INFO

Article history:
Received 8 February 2018
Received in revised form 18 April 2018
Accepted 26 April 2018
Available online 6 May 2018

Keywords:
PCB
Micropump
Lab on a chip
Electrolysis
Microfabrication
Interdigitated electrode

ABSTRACT

We report *for the first time* an electrolytic micropump based on an electrode chip fabricated on a printed circuit board (PCB), and compare its performance with that of a micropump based on an electrode chip fabricated using conventional microfabrication. Gold interdigitated (IDT) electrodes are patterned on a PCB to minimize ohmic loss during electrolysis. Custom-built acrylic fixtures are used to characterize pumping performance of various electrode chips with different electrode shapes and materials. Hydrogen and oxygen gas bubbles produced by electrolysis generate liquid flow inside a microchannel. As predicted by the theory of water electrolysis, the micropump produces flow rate increasing linearly with current at a wide range (1 mA–2 A). Our micropump yields the maximum flow rate of 31.6 ml/min and maximum backpressure of 547 kPa (at 34 μl/min), significantly high compared with the previous micropumps based on various actuation mechanisms including piezoelectric actuation, electroosmosis and phase change. The PCB-based micropump with a thick electroplated-gold electrode (0.43 μm) chip shows the overall best performance in terms of flow generation, power consumption and cost, compared with the PCB-based pump using an thin electroless-gold electrode (0.04 μm) and the pump using a microfabricated chip with a sputtered gold electrode (0.2 μm). We anticipate the PCB-based electrolysis pump will be used in portable lab-on-a-chip devices where an integrated microscale pressure source with low power consumption and simple fabrication is crucial.

1. Introduction

A self-contained, microscale, active pump has been an thriving area of research owing to its wide applications including LOC (Lab on a chip), biomedical microdevices (e.g., implantable drug dispenser), microelectronic-device cooling, miniaturized fuel cells and microhydraulics [1–10]. The LOC promises a rapid and sensitive analysis of biological and chemical analytes with minute reagent and sample consumption at low cost [11,12]. A micropump is an indispensable component of an LOC since it is essentially a pressure source driving liquids inside a network of microscale channels and fluidic components. However, many of LOCs still rely on a power-hungry external pressure source [13], sometimes inaccurate finger push [14] or tedious manual pipetting. Thus, a simple micropump that is monolithically fabricated and integrated into an LOC, and can deliver suitable pumping performance could be one of key ingredients for a wide success of the LOC.

Since 1970s when the first micropump was introduced [15], pumps of various actuation mechanisms, materials, shapes, form factors and figures of merit have been presented. Micropumps are usually classified based on ways to transfer momentum to liquid and characteristics of moving boundary [1,4]. A majority of micropumps published are “displacement” pumps consisting of a reciprocating diaphragm (solid) that is actuated piezoelectrically, electrostatically, thermopneumatically, etc. Having a periodically moving diaphragm, although some of these pumps yield excellent pumping performance, an intricate fabrication process including bonding of multiple thin-film layers and manual gluing of a piezoelectric film hinders facile integration into an LOC. Micropumps having rotational vanes (e.g., gear pump) share a similar drawback of manufacturing complexity. In order to overcome this limitation, “dynamic” micropumps in which direct, continuous momentum transfer to liquid generates flow have been proposed [1,10]. However, high operational voltage (electroosmotic, electrohydrodynamic), sensitivity to liquid and surface condition

* Corresponding author.
E-mail address: dohyun.kim@mju.ac.kr (D. Kim).

https://doi.org/10.1016/j.sna.2018.04.042
0924-4247/

(electroosmotic), limited selection of working fluids (electrohydrodynamic), and complex operation/fabrication and large current (magnetohydrodynamic) may have been the reasons that these pumps are not widely accepted as an integrable LOC component.

Other types of displacement micropumps based on phase change, electrowetting, or ferrofluids exploit aperiodic pressure gradient between driving fluid (liquid or gas) and immiscible working fluid [8]. These micropumps have generally simpler structures, thus leading to easier fabrication than the reciprocating-diaphragm micropumps do. Among the phase-change methods, electrolysis of water, an electrochemical conversion of liquid (water) to gas (hydrogen and oxygen) has drawn much attention as an actuation mechanism because of large volume expansion, high efficiency, excellent backpressure and low power consumption [16–19]. Moreover, since it only requires electrodes and electrolyte in a reservoir with no moving parts, simple construction and fabrication render an electrolytic micropump promising as an LOC pressure source [5,19,20].

Many different approaches were taken to improve the performance of electrolytic micropumps including electrode-design optimization [21,22], feedback control [23], parallelization [24], remote operation [25], protective electrode coating for enhanced lifetime [26], separation of electrolyte and working fluid [21,25,27–29] and bidirectional pumping [30]. All of these previous electrolytic micropumps have been fabricated on silicon or glass substrate using conventional microfabrication techniques [23,28,31–34]. However, microfabrication is costly and a cleanroom is not always accessible. On the other end of the spectrum, simple metal wires inserted in a reservoir were proposed as electrodes [35,36] but may result in reduced manufacturing precision and inferior reproducibility as these electrodes are manually assembled.

In order to address these issues of the previous electrolytic micropumps, we employ the printed-circuit-board (PCB) technology for fabrication. The PCB is an appealing platform for LOC devices because it has suitable manufacturing precision for microfluidic devices [37]. Various mechanical, electronic and electro-mechanical components can be assembled on a PCB [37,38]. Moreover, being a mature technology, many design tools are available to users and a PCB can be readily manufactured through well-standardized foundry services at low cost and in large volume. Application of the PCB technology to a microanalytical platform, so-called Lab-on-PCB has caught attention recently [36,37,39–42]. For a pressure source, there have been attempts to make reciprocating-diaphragm micropumps [43,44] and thermopneumatic pump [45] using the PCB technology. However, manual assembly of multiple PCB layers, heating wires, a piezo actuator and a diaphragm rendered device manufacturing too complex for wide-spread usage.

In order to see if a PCB-based electrolytic micropump has the potential to be used in portable LOC devices, we designed and fabricated PCB chips with interdigitated (IDT) gold electrodes for electrolysis. Pumping performance was analyzed in terms of flow rate and backpressure. We noted that the flow rate and backpressure are surprisingly high compared with the values published in recent review papers [1–10]. Lastly, we compared the performance of PCB-based micropumps with that of a microfabricated pump in terms of pumping efficiency, lifetime, cost and manufacturing accuracy.

2. Theory

2.1. Electrolysis as a pumping mechanism

When a voltage higher than the standard equilibrium voltage $V_{cell}{}^0 = 1.23$ V (1 atm, 25 °C) of two half-cell reactions (1) is applied to a pair of electrodes contacting aqueous solution at acidic or neutral pH, water molecule is electrochemically dissociated into hydrogen and oxygen molecules. An oxidation occurs by receiving two electrons from a water molecule to generate one half of oxygen gas molecule on anode. Simultaneously a reduction takes place on cathode by giving two electrons to two hydrogen ions to form a hydrogen gas molecule:

$$\begin{aligned} Anode &: H_2O(l) \leftrightarrow 2H^+(aq) + 2e^- + \frac{1}{2}O_2(g) \\ Cathode &: 2H^+(aq) + 2e^- \leftrightarrow H_2(g) \end{aligned} \quad . \tag{1}$$

The net reaction of water electrolysis is:

$$Net : H_2O(l) \rightarrow H_2(g) + \frac{1}{2}O_2(g) \ , \tag{2}$$

and the stoichiometric ratio of evolved gas to consumed liquid equals to 3:2. At a sufficiently high rate of gas evolution, electrolyte near the electrodes is supersaturated with the gas, and eventually gas bubbles are formed [20,46–48]. Theoretical volume expansion under isobaric condition was calculated by the ratio between liquid volume consumed and gas volume created through electrolysis: astounding ×1360 vol expansion [16]. Also, theoretical pressure generated under isochoric condition was as much as 200 MPa, superior to other common actuation mechanisms including piezoelectric and electromagnetic actuations [16]. Thus, electrolysis is well suited for the pumping mechanism where large volume expansion as well as high pressure are critical.

2.2. Flow rate

Assuming that current flowing through an electrolysis cell contributes to electrolysis 100%, the volume of generated gas V [m^3] is proportional to the total electrical charge C [C] consumed by the cell and can be expressed as follows [20]:

$$V = \frac{3V_m}{4F}C = \frac{3V_m}{4F}It \tag{3}$$

where V_m is the molar gas volume (24.7×10^{-3} m^3/mol at 1 atm, 25 °C), I the current [A] and F the faraday constant (96,485 C/mol). The flow rate Q [m^3/s] that a pump generates is equivalent to the rate of gas production:

$$Q = \frac{dV}{dt} = \frac{3V_m}{4F}I \ . \tag{4}$$

It is noted that the flow rate is proportional to the applied current if a constant-current mode (dc) is used. According to Eq. (4), the flow rate Q is about 10 μL/min under 1 atm when I is 1 mA [49], sufficient for common LOC applications.

2.3. Pumping efficiency

Efficiency of an electrolytic pump can be defined as the ratio of measured volume expansion to theoretical volume expansion [32]. For a constant-current mode and pumping duration t, the pumping efficient η can be expressed using flow rate Q:

$$\eta = \frac{V_{\text{experimental}}}{V_{\text{theoretical}}} = \frac{Q_{\text{experimental}} \times t}{Q_{\text{theoretical}} \times t} = \frac{Q_{\text{experimental}}}{Q_{\text{theoretical}}} \ . \tag{5}$$

The pumping efficiency is lower than 1 because not all currents contribute to gas production; some to nonfaradaic reaction such as double-layer charging, and side faradaic reaction such as electrode and adhesion-layer dissolution. In addition, there exist inevitable gas losses including gas recombination into water, gas dissolution and diffusion into neighboring electrolyte, and gas and electrolyte leakage [50].

2.4. Power consumption

An important consideration for a micropump integrated into a portable LOC device is to minimize power consumption. For constant-current operation, the consumed power of an electrolytic cell P_{cell} can be expressed as:

$$P_{cell} = IV_{cell} \ , \tag{6}$$

and the power can be reduced by decreasing cell voltage V_{cell}. The cell voltage is a sum of standard equilibrium voltage $V_{cell}{}^0$ and overvoltage V_{act}, V_{con} and V_{ohm}:

$$V_{cell} = V_{cell}^0 + V_{act} + V_{con} + V_{ohm} \ . \tag{7}$$

In order to drive electrolysis reaction in an appreciable rate for pumping, activation overvoltage V_{act} has to be applied to electrodes. This overvoltage is used to overcome the reaction energy barrier and highly depending on electrode materials and surface conditions. V_{act} shows a logarithmic relation with current. Platinum is commonly used as the electrode material owing to high catalytic activity and chemical inertness [51]. However, the platinum also shows a high catalytic activity on gas recombination into water [31]. Thus, we chose gold for chemical inertness [52] and material compatibility with the PCB manufacturing process. Concentration overvoltage V_{con} is related to mass transport and is increased when delivery of reactants to the electrode and removal of products from the electrode are slow. It is known that concentration overvoltage is much lower than ohmic and activation overvoltages [53]. The ohmic overvoltage is proportional to current I and the total ohmic resistance including cell resistance R_{cell}, bubble resistance R_{bubble} and circuit resistance $R_{circuit}$ [51]:

$$V_{ohm} = IR_{ohm} = I(R_{cell} + R_{bubble} + R_{circuit}) \ . \tag{8}$$

At a mild operating condition, bubble and circuit resistances can be negligible [54]. In this study, as a first-degree guideline for electrode design, we attempted to minimize cell resistance R_{cell} because (1) the activation overvoltage is not controllable since gold was selected as the electrode material owing to compatibility with the PCB process and chemical inertness; and (2) the concentration overvoltage, and the ohmic overvoltage caused by the bubble and circuit resistances were assumed to be small compared with the ohmic overvoltage caused by the cell resistance.

2.5. Minimizing cell resistance

A majority of electrolytic micropumps rely on IDT (interdigitated) electrode [20,23]. Its advantage over conventional microelectrode geometry (e.g., single band, circle) is a low cell resistance as it can minimize current path between anode and cathode by putting electrode pairs in close proximity using a periodical repetition of electrodes [55]. The cell resistance R_{cell} [Ω] can be expressed with the specific resistance of electrolyte ρ [Ω·m] and the proportionality factor called cell constant κ [m^{-1}]:

$$R_{cell} = \kappa\rho \ . \tag{9}$$

In our micropump, 1 M sodium-sulfate solution was used as the electrolyte [36,56] owing to low cost, low electroactivity and high electrical conductance (~91.1 mS/cm at 15% concentration) [57], that is, low specific resistance. The cell constant κ is determined by the shape of an IDT electrode, namely, W the width of a finger (band), S the space between two fingers, l_b the finger length and n_b the total number of fingers. Olthuis et al. derived expression for κ for an IDT electrode with more than 2 fingers [58]:

$$\kappa = \frac{1}{(n_b - 1)l_b} \frac{2K(k)}{K\left(\sqrt{1-k^2}\right)} \ , \tag{10}$$

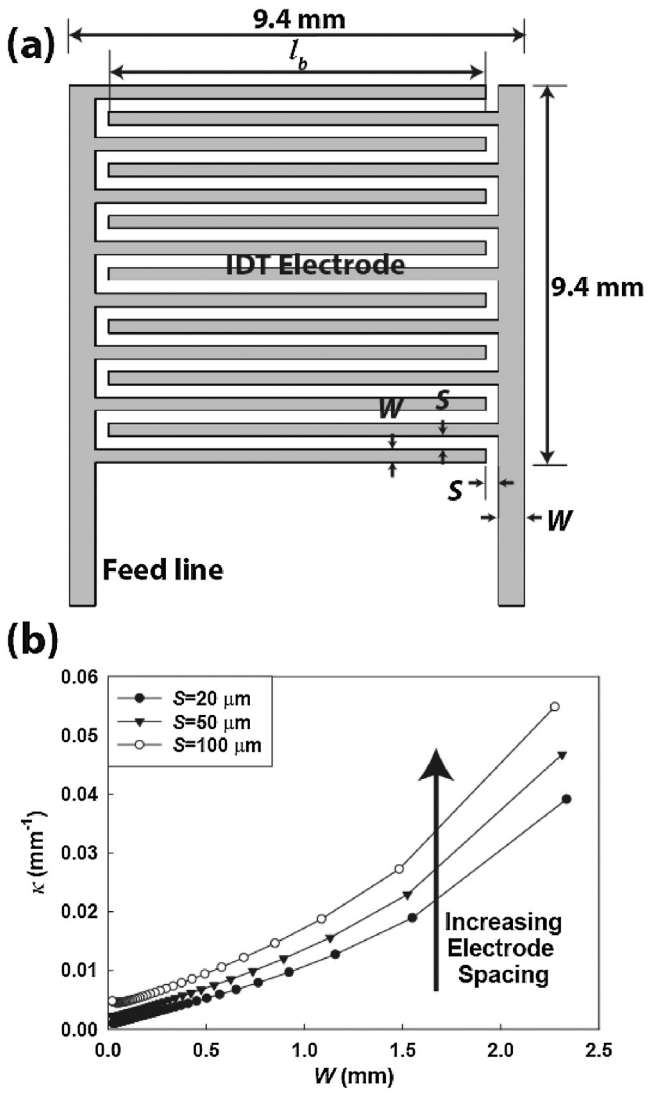

Fig. 1. (a) Layout and dimension of an IDT electrode, and (b) the cell constant κ as a function of electrode width W and spacing S calculated using a MATLAB code.

where the elliptic integral $K(k)$ and the modulus k are expressed as following:

$$K(k) = \int_{t=0}^{1} \frac{1}{\sqrt{(1-t^2)(1-k^2t^2)}} dt \ , \quad \text{and} \tag{11}$$

$$k = cos\left(\frac{\pi}{2}\frac{W}{S+W}\right) \ . \tag{12}$$

In our design, the footprint size of the IDT electrode was determined as $9.4 \times 9.4\,mm^2$ to fit in an electrolyte chamber. Therefore the finger length l_b was chosen to satisfy a geometric relationship:

$$l_b + 2S + 2W = 9.4 \ \ mm \,, \tag{13}$$

and the number of electrode n_b was chosen to satisfy another geometric relationship:

$$(n_b - 1)S + n_b W = 9.4 \ \ mm \,, \tag{14}$$

as seen in Fig. 1a. Using a MATLAB code, we calculated cell constant κ (Eq. 10) as a function of W for a constant electrode spacing S and for a number of fingers n_b (>2) satisfying the geometric relationship Eq. (14). Calculation was repeated for the three cases S = 20, 50 and 100 μm.

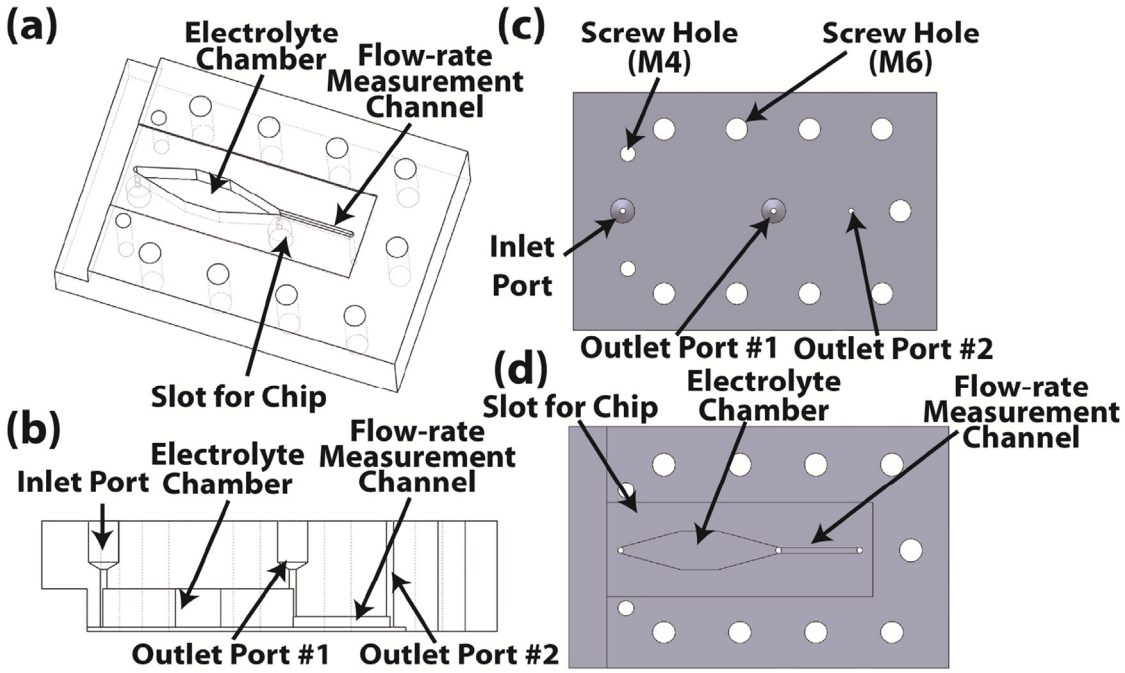

Fig. 2. A jig for measuring flow rate: (a) isometric view, (b) side view, (c) top view and (d) bottom view.

It was found that κ is a monotonically increasing function of W as seen in Fig. 1b and also increases with S. Consequently, we noted that the smallest W and S, the minimum feature size achievable in available PCB fabrication or microfabrication techniques, should be used in order to minimize R_{cell}. In addition, choosing the smallest S may increase the overall electrode area for electrolysis (Eq. 13) by increasing W and thus reduce R_{cell} (Fig. 1b). In Experimental section, three microfabricated electrode chips with different W and S values were tested to study an impact of the cell constant κ to the power consumption P_{cell}. For pumping-performance test of PCB electrode chips and their performance comparison with that of microfabricated chips, we chose $W = 100\ \mu m$ and $S = 100\ \mu m$ as it is the minimum achievable feature size of the PCB manufacturing service we employed.

3. Design and fabrication of micropumps

3.1. Jigs for testing flow rate and backpressure

A jig was designed to measure flow rate generated by microfabricated or PCB chips with different electrode shapes and materials (e.g., electroplated, electroless or sputtered gold). PMMA (poly methyl methacrylate) was used for the jig, owing to low gas permeability, transparency and good machinability. Fig. 2 shows a 3-D solid model for our jig. The top plate (length × width × height = 100 mm × 65 mm × 20 mm) houses a chamber (~1.4 ml) to store electrolyte solution and retain gas bubbles not to clog the flow-rate measurement channel. The tapered shape of the chamber enabled smooth transitions from the inlet port to the chamber and from the chamber to the flow-rate measurement channel. Inlet port and outlet port #1 were threaded so that 3-way cock valves (Diba Industries Inc., CT, USA) for injecting electrolyte and sealing the chamber were installed. Outlet port #2 was also threaded for connecting a tube to waste. Electrolyte was loaded into the chamber through Inlet port and then Outlet port #1, while Outlet port #2 was closed. In this way, only the chamber was filled with electrolyte and the electrolyte front was formed at the chamber exit, connected to the flow-rate measurement channel. The channel (21.4 mm × 1.5 mm × 2.5 mm) was used to visually measure flow rate. During measurement, Inlet port and Outlet port #2 were closed using the cock valves, but Outlet port #2 was open for venting. A ruler was affixed next to the channel to aid visual characterization of flow rate. The maximum flow rate about 32 ml/min (flow velocity = ~142 mm/s) was tested using this jig. High-speed video capture (400 frames per second) was good enough record a motion picture of flow. A slot (75 mm × 25 mm × 1 mm) was machined to clamp and replace a chip readily after use. As seen in Fig. 3, an IDT electrode chip is clamped between the top plate and the bottom plate (100 mm × 65 mm × 10 mm) and secured tightly using M4 and M6 screws. A gasket tape (Gore Series 500, W.L. Gore and Associates Inc., DE, USA) was attached to the both sides of the chip to minimize gas and electrolyte leakage.

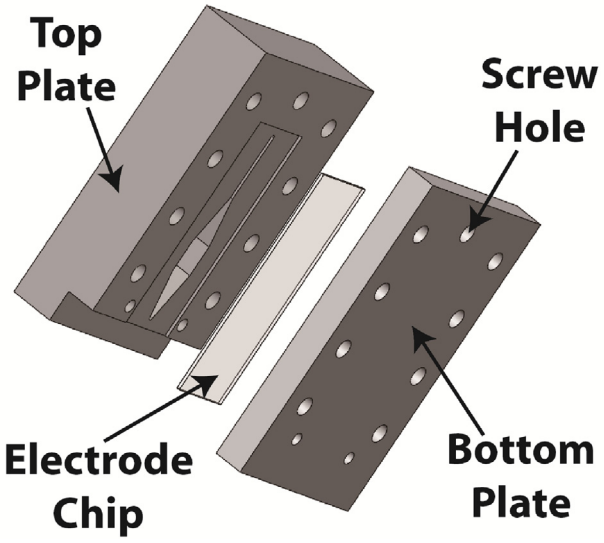

Fig. 3. An exploded view of an electrode chip clamped between the top and bottom plates.

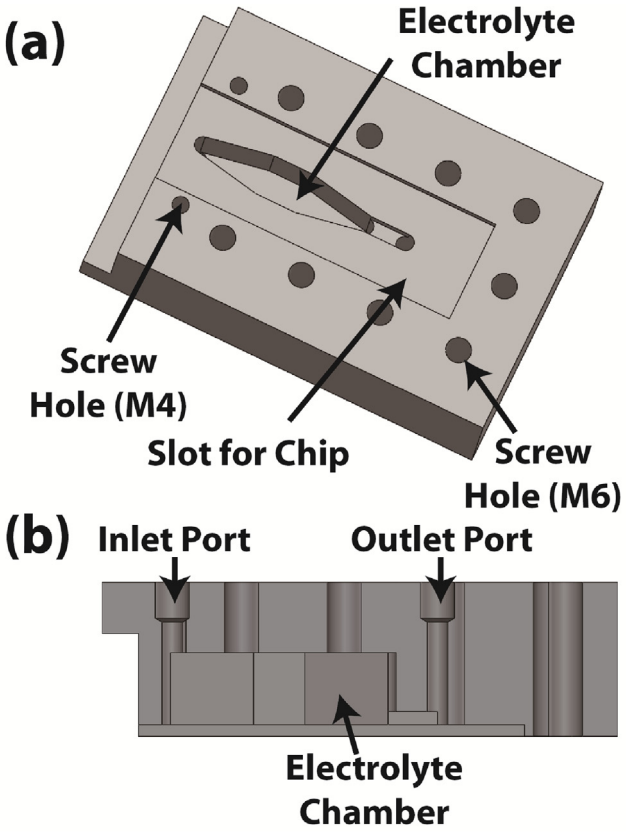

Fig. 4. A 3-D model of the second jig for backpressure measurement: (a) isometric view and (b) side view.

Table 1
Design parameters of microfabricated electrode chips.

Chip No.	W (μm)	S (μm)	Area (mm²)	SU-8 Insulation Layer
1	50	50	37.05	X
2	50	100	18.05	X
3	20	50	21.56	X
4	100	100	35.88	O

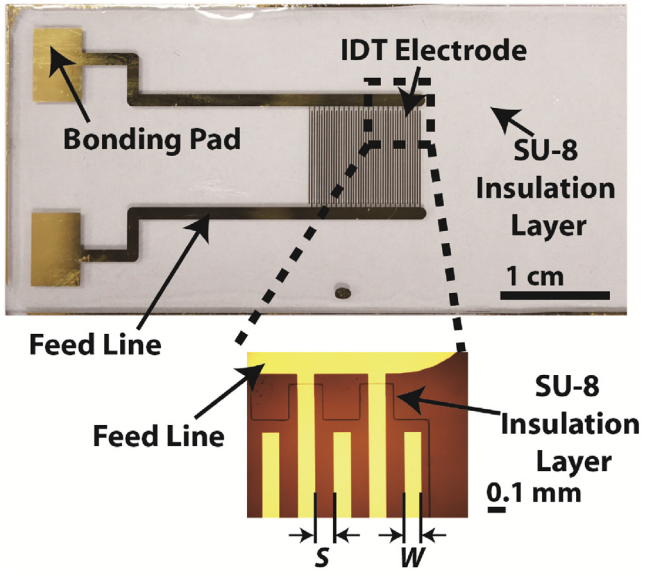

Fig. 5. Photograph of a microfabricated IDT chip with an SU-8 insulation layer. The inset figure shows electrode fingers (spacing *S* and width *W*), feed line and the SU-8 insulation layer.

For backpressure measurement, a similar but slightly different jig was designed (Fig. 4). The chamber volume was increased 3.5 times (i.e., 4.7 ml) for high-current experiment. An external in-line pressure sensor was connected to the jig for backpressure measurement. The flow rate was measured using an in-line flow sensor, not image analysis, because the channel would have been filled with the liquid to reach the external pressure sensor and the flow front end could have not been observed by a digital camera. Since the flow rate was not measured using the channel, its length was shortened (12 mm) and width was increased (4 mm) to reduce a pressure loss at high flow rates. In addition, Outlet port #1 was removed as there was no need to form the liquid front end at the exit of the electrolyte chamber. Removing the port also minimized gas and electrolyte leakage.

3.2. Microfabricated electrode chip

Two types of microfabricated chips were designed. The first type without an SU-8 insulation layer, was designed for studying an impact of cell constant on power consumption. An SU-8 insulation layer was added to the second type because we noticed a short lifetime of the first type without a proper feed-line protection. The second type was also used for performance comparison with PCB electrode chips, and flow-rate and backpressure measurements at high currents (up to 2 A).

For the first type, the IDT electrodes of three different dimensions were designed (Chip No. 1–3 in Table 1). The electrodes were patterned on a gold-coated glass slide (75 mm × 25 mm × 1 mm) using a standard lithography process. Briefly, a thin-film gold of 200 nm was sputtered on thoroughly cleaned glass slides with 20-nm titanium adhesion layer using a foundry service (Korea Advanced Nano Fab Center, Suwon, South Korea). A positive photoresist GXR-601 (14 cp, AZ Electronic Materials, Luxembourg) was used as an etch mask for wet etching after photolithography and development (AZ 300 MIF, AZ Electronic Materials). IDT-electrode patterns were obtained by timed wet etching of gold using TFA etchant (8 wt% iodine, 21 wt% potassium iodide, 71 wt% water, Transene Company Inc., MA, USA), and subsequent etching of the titanium adhesion layer using TFTN etchant (HCl based, Transene Company Inc.). After etching, the photoresist was stripped using acetone.

The second type of the microfabricated chip has identical electrode width and spacing of 100 μm (Chip No. 4, Table 1). Nano SU-8 (Formulation 2, Microchem, MA, USA) was used to cover feed line and exposed glass surface. The SU-8 was chosen because of film robustness and easy fabrication [59]. Lithography process was optimized to form a 5.7-μm-thick SU-8 insulation layer with proper adhesion to gold and glass surfaces. A calibrated wafer-inspection microscope (LEICA INM-100, Leica, Wetzlar, Germany) was used to characterize the accuracy of microfabrication performed in our cleanroom (Semiconductor Process Diagnosis Research Center at Myongji University, South Korea). The manufacturing error, an average dimensional deviation from the designed electrode width *W* (measured at five different locations of five samples) was about 3.72 μm. Fig. 5 shows a photograph of a microfabricated electrode chip of the second type. The magnified photo shows electrode fingers, feed lines and an SU-8 insulation layer.

3.3. PCB electrode chip

PCB electrode chips were designed using OrCAD software (Cadence Design Systems, CA, USA), and fabricated using a local PCB foundry service (Hansaem Digitec, South Korea). Considering the manufacturing specification of the foundry service, electrode

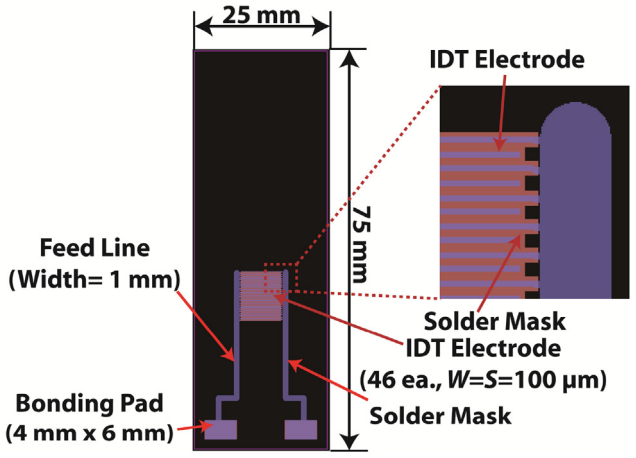

Fig. 6. A layout of a PCB electrode chip. The inset figure shows detailed electrode-finger and solder-mask design.

width and spacing were determined as 100 μm (i.e., W = 100 μm, S = 100 μm, identical to Chip No. 4, Table 1). In order to accommodate an IDT electrode within the given footprint of 9.4 × 9.4 mm^2, the number of electrode fingers (n_b) was determined to be 46, and the total electrode area was 35.88 mm^2. Pad Designer in the OrCAD package was used to design electrode fingers, bonding pads and solder-mask (a lacquer-like polymer layer for insulation) features. PCB Editor was used to connect between electrode fingers, feed lines and bonding pads (Fig. 6).

Fig. 7a shows the photograph of a fabricated PCB electrode chip. Two types of PCB chips were fabricated with the same layout: one with an electroplated gold film (Fig. 7b) and the other with an electroless gold film (Fig. 7c). Detailed fabrication process of a PCB can be found elsewhere [60]. Briefly, 1-mm-thick FR-4 (fiberglass-reinforced epoxy laminate material), coated with 16.87-μm-thick copper foil, was laminated with a photoresist dry film. After photolithography and dry-film development, the copper foil is selectively removed by wet etching. After the dry film is stripped, a solder mask is patterned to protect copper traces. Exposed copper surfaces (electrode fingers and bonding pads) are plated with gold using two methods: (1) In the ENIG (Electroless Nickel Immersion Gold) process, nickel is autocatalytically electroplated on the copper surface, and then nickel atoms are displaced by gold atoms to form a thin layer [61]; and (2) In the "hard gold" process, a gold layer is electroplated on an electroplated nickel adhesion layer. Fig. 7b and 7c show thickness of metal layers characterized by a measurement service (AUtech, South Korea) using a dissected PCB cross section. The inset figure of Fig. 7a shows a magnified photo of electrode fingers taken using the inspection microscope (Leica INM 100). It was noted that the feed line were well protective by the solder mask. The manufacturing error for the electroless-gold-electrode chip was measured (at five different locations of five samples), and it was about 1.97 μm. The manufacturing error of the electroplated-gold-electrode chips was about 4.51 μm.

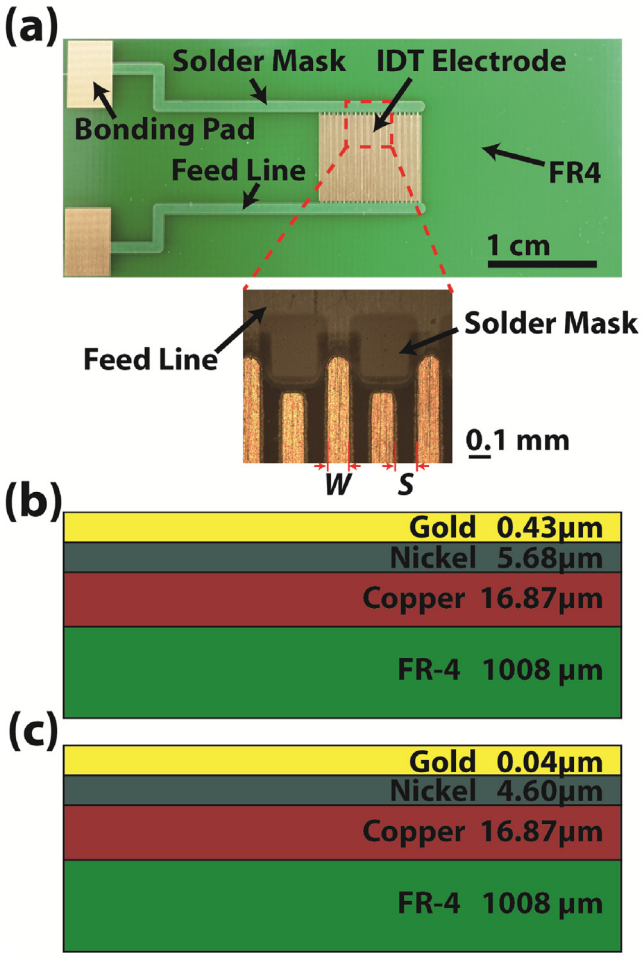

Fig. 7. PCB electrode chips: (a) A photograph of a PCB chip and a magnified figure of electrode fingers (spacing S and width W), a feed line and a solder mask; (b) A layer diagram of the PCB chip with electroplated gold electrode; (c) A layer diagram of the PCB chip with electroless gold electrode.

4. Experimental

4.1. Experimental set up for flow-rate measurement

Fig. 8 shows a schematic diagram and a photograph of the experimental setup for flow-rate measurement of our micropumps. An electrode chip, attached with sealing tapes, was tightly clamped in the PMMA jig using screws. For visualization, solution of 1 M sodium sulfate with a red food-color dye was injected into the jig using a syringe pump (Legato 100, KD Scientific Inc., MA, USA); the electrolyte chamber and flow-rate measurement channel can be easily noticed in the inset figure of Fig. 8b. After electrolyte was injected, the both cock valves were tightly closed to prevent leakage, but the vent is left open for liquid flow. A precision source meter (B2901A, Keysight Technologies, CA, USA) was used to apply constant current (1 mA–2 A). The cell voltage V_{cell} and the power consumption P_{cell} was measured accurately using the source meter.

Gas bubbles were generated by electrolysis and trapped inside the electrolyte chamber because the bubbles tends to float and the height of the chamber is larger than that of the measurement channel (5 mm vs. 2.5 mm). Pressurized electrolyte rushed through the microchannel, connected to the vent (Outlet port #2, atmospheric pressure). The front end of running flow was then recorded with the ruler situated next to the channel, using a high-speed digital camera. The recorded motion picture was analyzed using an open-source image-analysis software ImageJ (National Institute of Health, MD, USA). A PC was used to control all the electronics including the syringe pump, source meter and digital camera. Microfabricated chips with various electrode shapes and PCB electrode chips with different gold films were tested in this experimental setup for flow-rate measurement. Temperature was 23 ± 1 °C during the measurement.

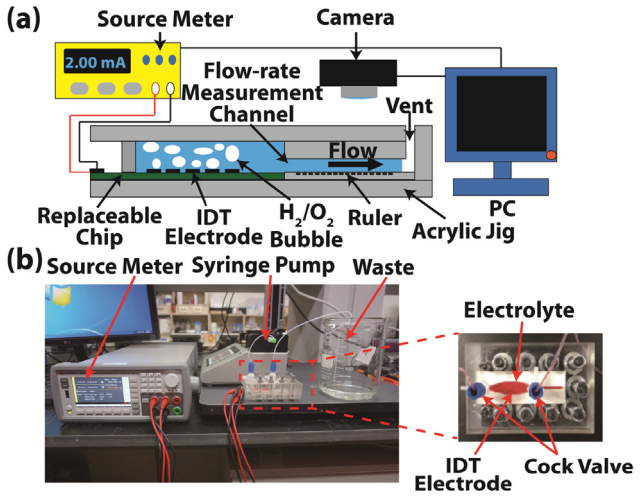

Fig. 8. The experimental setup for flow-rate measurement: (a) a schematic diagram and (b) a photograph (the inset figure shows top view of the PMMA jig with red-colored electrolyte for visualization) (For interpretation of the references to color in this figure legend, the reader is referred to the web version of this article).

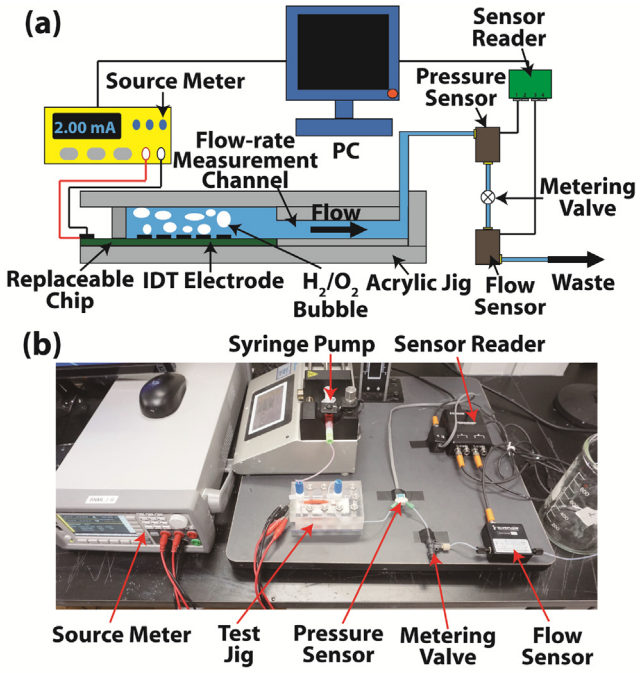

Fig. 9. The experimental setup for backpressure measurement: (a) a schematic diagram and (b) a photograph.

4.2. Experimental set up for backpressure measurement

In order to assess the capability to drive liquid through a complicated network of microscale channels, backpressure was measured. For backpressure measurement, a new experimental setup was also made as seen in Fig. 9. Major differences from the flow-rate measurement setup are: (1) Electrolysis was performed in the second type of PMMA jig (Fig. 4); and (2) An external in-line flow sensor (MFS-5, Elveflow, France) was used for flow-rate measurement instead of image analysis. A micro metering valve (P-446, IDEX Health & Science, WA, USA) was used to control backpressure, which was then measured using an external in-line pressure sensor (MPS-5, Elveflow). All the fluidic components were linked using 1/16-inch Teflon tubing. The both sensors were connected to

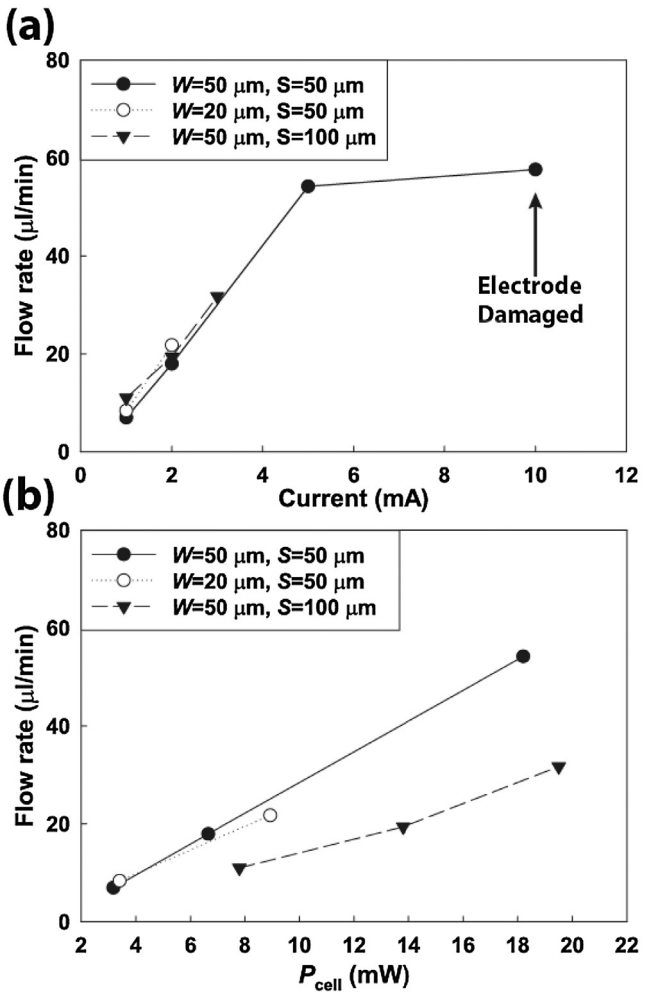

Fig. 10. Performance characterization of microfabricated electrode chips: (a) flow rate as a function of input current and (b) flow rate as function of power consumption.

a sensor reader (MSR, Elveflow), connected to the control PC for data acquisition. Only the PCB chip with the electroplated gold electrode was tested using the backpressure-measurement setup because of its better pumping performance than other types of electrode chips.

A knob of the metering valve was set to a predetermined position and a constant current was applied (0.1–2 A). Flow rate and backpressure were simultaneously recorded as a function of time. It was noted that flow rate and pressure values surged in the beginning of electrolysis, and became a steady state later. The pressure value dropped back to atmospheric pressure slowly when the current was turned off. We determined backpressure by averaging pressure values at this steady-state region.

5. Result

5.1. Characterization of the micropump using microfabricated electrode chips

Three different microfabricated electrode chips (Chip No. 1–3 in Table 1) were tested using the flow-rate-measurement setup (Fig. 8). Fig. 10a shows that flow rate linearly increases with input current according to Eq. 4, except the 10-mA case ($W = 50\,\mu m$, $S = 50\,\mu m$) where electrode degradation was observed after the experiment. Flow rates for the same input current are very similar regardless of electrode geometry. Fig. 10b shows that power consumption is largest for the chip with $W = 50\,\mu m$ and $S = 100\,\mu m$

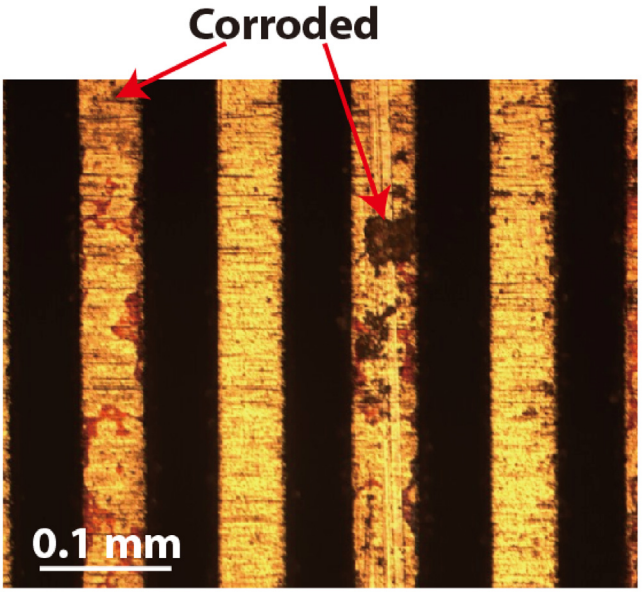

Fig. 11. Electrochemically damaged IDT-electrode fingers of a microfabricated electrode chip ($W = 50\ \mu m$, $S = 50\ \mu m$).

where the cell constant is largest ($k = 0.00453\ mm^{-1}$). Power consumption of the chips with similar cell constants ($0.0022\ mm^{-1}$ for $W = 20\ \mu m$ and $S = 50\ \mu m$, and $0.0023\ mm^{-1}$ for $W = 50\ \mu m$ and $S = 50\ \mu m$) was analogous. Consequently, we noted that the cell resistance R_{cell} is a major factor affecting power consumption (Eqs. (6)–(9)) under the given experimental condition.

The microfabricated electrode chips can only be used 2–4 times, indicating short lifetime. We inspected the chips after being malfunctioned; the feed lines and electrode fingers were delaminated from the glass substrate owing to electrochemical damage on the titanium adhesion layer as can be seen in Fig. 11. Such electrochemical damage on gold or platinum electrodes are well documented in literature [21,24,47,50]. The electrode damage may reduce pumping efficiency, but a damage to the feed line can completely terminate electrolysis reaction. The reason that the flow rate at 10 mA is much less than expected value assuming a linear increase ($W = 50\ \mu m$, $S = 50\ \mu m$ case) was due to electrode delamination. In order to extend the lifetime, the feed line was insulated using an SU-8 layer [59] for the second type of microfabricated chips, which will be detailed in Section 5.3.

Pumping efficiency η was lower than 1 and increased with the input current of 1–5 mA (Fig. 12, $W = 50\ \mu m$, $S = 50\ \mu m$). As described earlier (Section 2.3), not all currents may have contributed to gas production. Gases may have been lost owing to gas recombination, gas dissolution and diffusion into electrolyte, and gas leakage. It is thought that the value of η increases with the input current because the volume loss owing to gas recombination, and gas diffusion and dissolution becomes relatively insignificant as the rate of gas production increases [50].

5.2. Characterization of the micropump using PCB electrode chips

The foundry-processed PCB electrode chips (electroless or electroplated gold) were tested using the same test setup under the same experimental condition. The lifetime of the PCB chips is much longer than microfabricated chips *without* the SU-8 layer; the feed line was intact even after 6–7 runs. Also, the flow rate of the PCB chips was linear throughout tested current range of 1–10 mA, whereas the flow rate fell off at 10 mA for the microfabricated chip owing to electrode delamination.

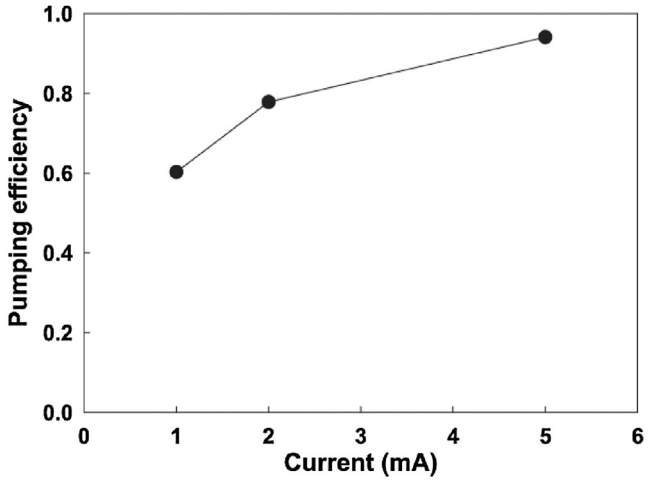

Fig. 12. Pumping efficiency as a function of input current (the microfabricated chip with electrode geometry $W = 50\ \mu m$ and $S = 50\ \mu m$).

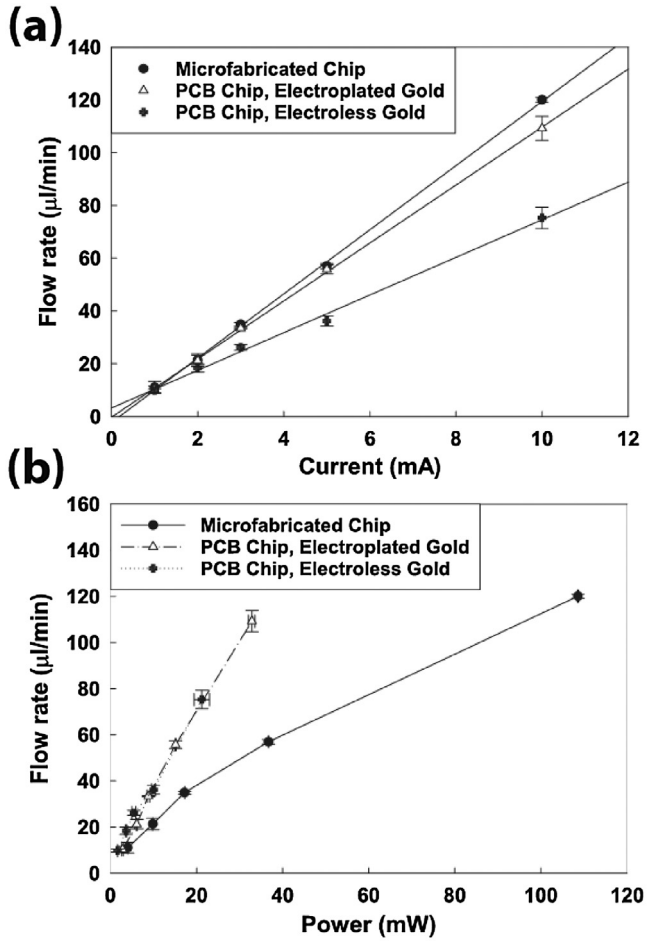

Fig. 13. Performance comparison between PCB electrode chips (electroless or electroplated golds) and microfabricated chip: (a) flow rate as a function of current and (b) flow rate as a function of power consumption.

In order to examine the potential of PCB-based electrolytic micropumps, we sought to compare performance of the PCB chips (electroless and electroplate gold) with that of the microfabricated chips having the same design (Fig. 6) and an SU-8 insulation layer for feed-line protection. As can be seen in Fig. 13, flow rate of the PCB chips with electroplated gold was 10.2–109.2 μl/min

Table 2
Performance comparison of the three types of electrode chips, (a) the microfabricated chip, (b) the PCB chip with electroless gold and (c) the PCB chip with electroplated gold electrode.

	PPI (μl/C)	Linearity (R^2)	Lifetime (min)	Manufacturing error (μm)	Cost ($)
Microfabricated	200.1	0.998	63.9	3.72	322
PCB (electroless gold)	130.7	0.994	11.3	1.97	10
PCB (electroplated gold)	184.5	0.999	30.6	4.51	19

(power consumption of 2.8–32.9 mW) and that of the PCB chips with electroless gold was 9.8–75.3 μl/min (power consumption of 1.6–21.2 mW). For the microfabricated chips, flow rate was 11.0–120.1 μl/min (power consumption of 4.0–108.6 mW). Comparison results are summarized in Table 2.

Pumping performance index (PPI) is defined as the slope of a flow rate vs. current curve (Fig. 13a), essentially volume expansion per electrical charge consumed during electrolysis. The microfabricated chips with an SU-8 insulation layer shows slightly higher PPI than the PCB chip with electroplated gold (7.8%), and much higher PPI than the PCB chip with electroless gold (34.7%) as seen in Table 2. As the nominal area of the IDT electrode is same for these three types of chips and the same current is applied, the nominal current density should be equal. However, exposed side walls of an IDT electrode also provide additional surface area for electrolysis. Fig. 7b and 7c show that the side-wall heights of the electroplated and electroless gold electrodes of the PCB chips are much larger than that of the microfabricated chip (22.98 μm and 21.51 μm vs. 0.22 μm). Nickel and copper present in the PCB electrodes also have high catalytic activities on electrolysis [51]. Therefore, the actual current density should be larger for the microfabricated chip, resulting in a higher rate of gas evolution [46,48,50,51,62]. Nevertheless, the reason that the PCB chip with electroless gold electrode shows lower flow rates than that of the PCB chip with electroplated gold is not well understood. It is speculated that faster degradation of the electroless-gold electrode, evidenced by shorter life time (Table 2), may be attributed to the lower flow rates, probably owing to a thin ENIG gold layer (40 nm vs. 430 nm). As seen in Fig. 13b, power consumption of the PCB chips was observed to be significantly lower (almost three times) than that of the microfabricated chip for a given flow rate. Having the same nominal electrode area but much taller side walls, the cell resistance R_{cell} of the PCB chips should be lower, and circuit resistance $R_{circuit}$, impeding current through feed lines and electrode fingers, should be lower as well. The linearity (R^2 value) between input current and flow rate was close to 1 for the all types of electrode chips (Table 2), indicating that the linear relationship of Eq. (4) holds well as long as the electrode chips are not damaged significantly.

In addition to the PPI, we compared auxiliary performance characteristics of the three types of electrode chips in Table 2. Lifetime is defined as the longest time that an electrode chip generates a stable flow rate under application of 1-mA constant current. The PCB chip with electroless gold electrode yielded the shortest lifetime, and the PCB chip with electroplated gold was next, probably owing to the thin ENIG layer. However, rather surprisingly, the microfabricated chip with SU-8 insulation layer showed the lifetime almost twice longer than that of the PCB chip with almost twice thicker gold layer. The shorter lifetime of the PCB chips could be attributed to electrochemical damage on copper and nickel layers [18]. As described earlier, manufacturing error is defined as the average value of absolute difference between the measured and nominal electrode width (W) of five chips, measured at five different locations. Notably, the well-established PCB process shows a similar manufacturing error (1.97 μm and 4.51 μm for the PCB chips with electroless and electroplated gold, respectively) with that of microfabrication performed in our cleanroom, which may have not been fully optimized (3.72 μm). It is noted from this work that process optimization is important to achieve accurate microfabrication.

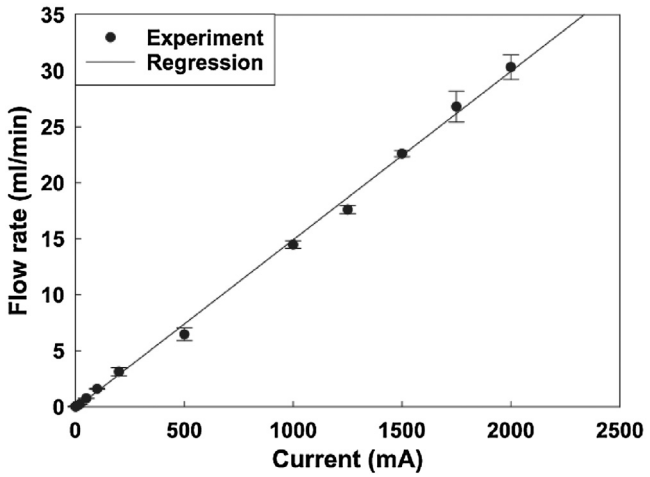

Fig. 14. Flow rate as a function of input current for the PCB chip with electroplated gold electrode.

Lastly, we compared the costs of manufacturing electrode chips. For the cost of microfabricated chips, photomask-manufacturing cost, gold-sputtering service fee, cleanroom fee, labor cost and all material costs were counted per chip. For the PCB chips, foundry-service fee was divided by the number of chips. The cost of the PCB chips were 17 or 32 times lower than the microfabricated chips. Considering PPI, power consumption, lifetime, manufacturing error and cost, the PCB chip with electroplated gold was deemed the overall best performing chip for application in a portable LOC device. Consequently, we sought to further analyze the pumping performance of the PCB chip with electroplated gold electrode.

5.3. Performance analysis of the PCB chip with electroplated gold electrode

Deemed promising, we examined the pumping performance of the PCB chip with electroplated gold electrode to its limit. For flow-rate measurement, the input current was increased up to 2 A. It was observed that the lifetime of the chip reduces as the current increases; the IDT electrodes failed immediately for a current larger than 2 A. An excellent maximum flow rate of 31.6 ml/min at 2 A (the average flow rate: 30.3 ml/min) was observed as seen in Fig. 14. The flow rate shows a linear relationship with current in the given current range (R^2 = 0.997). The flow rate of our micropump was the third highest, based on the review papers we studied [1–10], chasing the electroosmotic pump by Yao et al. [63] (flow rate of 33 ml/min) and the reciprocating-diaphragm pump by Kim et al. [64] (flow rate of 32.9 ml/min). The micropump by Kim et al. was piezoelectrically actuated using 150-V square-wave voltages at 300 Hz. 100-V dc voltage was required for the electroosmotic pump by Yao et al. In contrast, our operational voltage was mere 5.9 V for the maximum flow rate of 30.3 ml/min, which is advantageous to be used in a portable LOC device. Moreover, complex

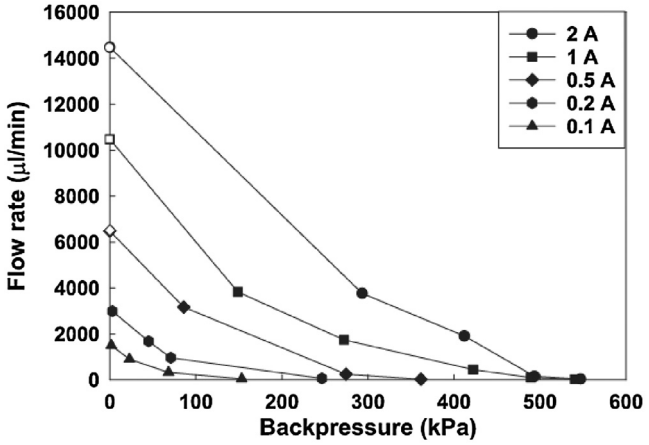

Fig. 15. Flow rate of the PCB chip with electroplated gold electrode as a function of backpressure. The empty symbols indicate data measured in the flow-rate measurement jig (Fig. 2) and experimental setup (Fig. 8) assuming zero backpressure.

and costly porous frit or nanochannel fabrication is required for the electroosmotic pumps [65].

We also sought to compare our pump to previous electrolytic pumps. PPI values of the previous pumps were estimated using published flow rate vs. current data [20,21,24,31,34–36,50]. As long as a constant current is applied, flow rate is proportional to the current, predicted by Eq. (4), but is less than calculated value owing to various gas losses and low current density. Depending on experimental conditions including electrode geometry, electrode material and electrolyte, the PPI values lie between 76.8–193 μl/C, equivalent to 41.7–104.8% of the PPI of the PCB chip with electroplated gold electrode. The values are not drastically different from our results. However, the maximum flow rates reported previously are much smaller (0.19–141.4 μL/min) than ours (31.6 ml/min). A major difference could be that much larger current can be applied (A vs. μA∼ mA) in our PCB pump, thanks to the longer lifetime.

The significantly high flow rate was achieved, but the test was performed under near-zero backpressure condition as seen in the schematic diagram of the experimental setup (Fig. 8). An LOC device usually consists of a network of long microchannels. Therefore the capability to overcome backpressure has been of a great interest for an integrable micropump. Using the second jig (Fig. 4) and experimental setup (Fig. 9), backpressure was measured by applying constant current of 0.1–2 A. Fig. 15 shows the relationship between backpressure and flow rate. It should be noted that the first jig (Fig. 2) was used for zero-backpressure data for the 0.5–2 A cases (indicated by empty symbols) owing to a measurement limit of the flow sensor MFS-5 (i.e., 5 ml/min). Pressure-generation performance was also outstanding: maximum 547 kPa (∼5.4 atm) at the flow rate of 34 μl/min. As can be seen in all the backpressure vs. flow rate curves, the flow-rate reduction worsened at higher backpressure, considering ideal curves represented by straight lines [66,67]. It is speculated that pressure loss owing to gas recombination into water, gas dissolution and diffusion into electrolyte exacerbates at a high backpressure [50]. Electrolyte leakage though the jig, fluidic fittings and couplings were readily observed at a high pressure (e.g., >200 kPa) and may be a cause of reduction in flow rate. We also compared the measured backpressure with the published values in the review papers [1–10]. Electroosmotic micropumps yielded outstanding backpressure at the cost of exceptionally high operational voltages: 11 MPa at 2 kV [68] and 2 MPa at 5 kV [69]. Volume expansion by phase change of paraffin generated 0.9 MPa but at orders-of-magnitude-lower flow rate (74 nL/min) than our micropump was obtained [70]. To best of our knowledge, our micropump yielded the best backpressure except those three cases.

In summary, our PCB-based electrolytic micropump achieved a top-tier pumping performance in comparison with the published micropumps often relying on high operation voltages, intricate and costly fabrication techniques, and yielding inferior flow rates. The established and affordable PCB technology may be well-suited to fabricate a micropump for a portable LOC device, comparing with a pump using a microfabricated electrode chip, in terms of flow generation, power consumption, lifetime and cost.

6. Conclusions

Much efforts have been made to develop a microscale pump with high flow rate, backpressure, energy efficiency, and yet low cost and simple fabrication because it is an indispensable component for various applications including lab on a chip (LOC), microelectronics cooling and microhydraulics. A large body of literature and commercialization efforts have been focused on reciprocating-diaphragm micropumps based on piezoelectric actuation, but high actuation voltage, pulsating flow, and, most of all, complicated microfabrication process may have been major roadblocks to wide adaptation in LOC devices, especially for portable applications. Numerous, scientifically intriguing pumping mechanisms have been suggested to overcome the limitations but they are not free of drawbacks including complicated operation, high power consumption and input voltage, low flow rate, irreplicable pumping rate control, and complex fabrication.

Structure, operation and fabrication of an electrolytic micropump are usually simpler than other types as requiring only electrodes and electrolyte for generation of flow. In addition to ordinary flow-rate performance, one limitation of the previous electrolytic pumps was expensive and hard-to-access cleanroom-based microfabrication. We opted to use the PCB technology for fabrication because it allows mature, affordable, straightforward foundry-based manufacturing. In our study, the PCB chip with electroplated IDT gold electrode was an excellent choice for a micropump, considering overall flow generation, power consumption, durability, manufacturing error and cost. Our PCB-based micropump yielded an outstanding flow rate up to 31.6 ml/min and backpressure up to 547 kPa with a mild input voltage ranged 1.7–5.9 V, which are significantly high performance compared with previous micropumps of various actuation mechanisms including electrolytic pumps. A microfabricated chip with sputtered-gold electrodes and an SU-8 insulation layer was better than the PCB counterpart in terms of lifetime and volume generation (i.e., PPI). However, it may not be well suited for portable LOC applications where cost and power consumption are of concern.

Another notable advantage of the PCB technology over the conventional microfabrication is versatility to incorporate a large collection of electronic, electric and electromechanical components, and scalability to form a complex microfluidic system for multistep bioassays. We are currently working to build a portable PCB-based LOC system integrated with a CMOS impedance microarray for DNA and protein analysis and with our electrolytic micropumps for flow control. We foresee in near future that PCB-based micropumps are used in a wide range of LOC applications where low voltage, low power consumption, low cost, high pumping rate and lastly simple electric control of fluids are important.

Acknowledgements

This material is based upon work supported by the MOTIE (Ministry of Trade, Industry & Energy of the Republic of Korea) under Industrial Technology Innovation Program, No.10052106, ‘Development of CMOS/MEMS hybrid biosensor array platform’.

This work was also supported by the Korea Institute of Energy Technology Evaluation and Planning (KETEP) and the MOTIE (No. 20174010201160).

References

[1] D.J. Laser, J.G. Santiago, A review of micropumps, J. Micromech. Microeng. 14 (2004) R35–R64.
[2] K.-S. Yun, E. Yoon, Micropumps for MEMS/NEMS and microfluidic systems, in: C.T. Leondes (Ed.), MEMS/NEMS Handbook Techniques and Applications, Springer, New York, 2006, pp. 1112–1144.
[3] F. Amirouche, Y. Zhou, T. Johnson, Current micropump technologies and their biomedical applications, Microsyst. Technol. 15 (2009) 647–666.
[4] B.D. Iverson, S.V. Garimella, Recent advances in microscale pumping technologies: a review and evaluation, Microfluid. Nanofluid. 5 (2008) 145–174.
[5] P. Woias, Micropumps—past, progress and future prospects, Sens. Actuators B Chem. 105 (2005) 28–38.
[6] A. Nisar, N. Afzulpurkar, B. Mahaisavariya, A. Tuantranont, MEMS-based micropumps in drug delivery and biomedical applications, Sens. Actuators B Chem. 130 (2008) 917–942.
[7] A.K. Au, H. Lai, B.R. Utela, A. Folch, Microvalves and micropumps for BioMEMS, Micromachines 2 (2011) 179–220.
[8] N.-T. Nguyen, X. Huang, T.K. Chuan, MEMS-micropumps: a review, J. Fluids Eng. 124 (2002) 384–392.
[9] S. Yokota, A review on micropumps from the viewpoint of volumetric power density, Mech. Eng. Rev. 1 (2014) 1–14.
[10] X. Wang, C. Cheng, S. Wang, S. Liu, Electroosmotic pumps and their applications in microfluidic systems, Microfluid. Nanofluid. 6 (2009) 145–162.
[11] G.M. Whitesides, The origins and the future of microfluidics, Nature 442 (2006) 368–373.
[12] A. Manz, N. Graber, H.M. Widmer, Miniaturized total chemical analysis systems: a novel concept for chemical sensing, Sens. Actuators B Chem. 1 (1990) 244–248.
[13] D. Mark, S. Haeberle, G. Roth, F. Von Stetten, R. Zengerle, Microfluidic lab-on-a-chip platforms: requirements, characteristics and applications, in: S. Kakac, B. Kosoy, D. Li, A. Pramuanjaroenkij (Eds.), Microfluidics Based Microsystems Fundamentals and Applications, Springer, New York, 2010, pp. 305–376.
[14] K. Iwai, K.C. Shih, X. Lin, T.A. Brubaker, R.D. Sochol, L. Lin, Finger-powered microfluidic systems using multilayer soft lithography and injection molding processes, Lab Chip 14 (2014) 3790–3799.
[15] J.L. Thomas, S. Bessman, Prototype for an implantable micropump powdered by piezoelectric disk benders, Trans. Am. Soc. Artif. Intern. Organs 21 (1975) 516–522.
[16] C.G. Cameron, M.S. Freund, Electrolytic actuators: alternative, high-performance, material-based devices, Proc. Natl. Acad. Sci. U. S. A. 99 (2002) 7827–7831.
[17] W. Kempe, W. Schapper, Electrochemical actuators, in: International Conference on New Actuators, 1990, pp. 162.
[18] C.R. Neagu, J.G. Gardeniers, M. Elwenspoek, J.J. Kelly, An electrochemical microactuator: principle and first results, J. Microelectromech. Syst. 5 (1996) 2–9.
[19] D. O'Keefe, C. O'herlihy, Y. Gross, J. Kelly, Patient-controlled analgesia using a miniature electrochemically driven infusion pump, Br. J. Anaesth. 73 (1994) 843–846.
[20] S. Böhm, W. Olthuis, P. Bergveld, An integrated micromachined electrochemical pump and dosing system, Biomed. Microdevices 1 (1999) 121–130.
[21] P.-Y. Li, R. Sheybani, C.A. Gutierrez, J.T. Kuo, E. Meng, A parylene bellows electrochemical actuator, J. Microelectromech. Syst. 19 (2010) 215–228.
[22] V.F. Lvovich, C. Liu, M.F. Smiechowski, Optimization and fabrication of planar interdigitated impedance sensors for highly resistive non-aqueous industrial fluids, Sens. Actuators B Chem. 119 (2006) 490–496.
[23] S. Böhm, B. Timmer, W. Olthuis, P. Bergveld, A closed-loop controlled electrochemically actuated micro-dosing system, J. Micromech. Microeng. 10 (2000) 498–504.
[24] V.I. Furdui, J.K. Kariuki, D.J. Harrison, Microfabricated electrolysis pump system for isolating rare cells in blood, J. Micromech. Microeng. 13 (2003) S164–S170.
[25] Y. Yi, A. Zaher, O. Yassine, J. Kosel, I.G. Foulds, A remotely operated drug delivery system with an electrolytic pump and a thermo-responsive valve, Biomicrofluidics 9 (2015) 052608.
[26] R. Sheybani, E. Meng, Acceleration techniques for recombination of gases in electrolysis microactuators with Nafion®-coated electrocatalyst, Sens. Actuators B Chem. 221 (2015) 914–922.
[27] T. Stanczyk, B. Ilic, P.J. Hesketh, J.G. Boyd, A microfabricated electrochemical actuator for large displacements, J. Microelectromech. Syst. 9 (2000) 314–320.
[28] C. Lui, S. Stelick, N. Cady, C. Batt, Low-power microfluidic electro-hydraulic pump (EHP), Lab Chip 10 (2010) 74–79.
[29] S.W. Lee, W.Y. Sim, S.S. Yang, Fabrication and in vitro test of a microsyringe, Sens. Actuators A Phys. 83 (2000) 17–23.
[30] H. Suzuki, R. Yoneyama, A reversible electrochemical nanosyringe pump and some considerations to realize low-power consumption, Sens. Actuators B Chem. 86 (2002) 242–250.
[31] R. Sheybani, H. Gensler, E. Meng, A MEMS electrochemical bellows actuator for fluid metering applications, Biomed. Microdevices 15 (2013) 37–48.
[32] P.-Y. Li, J. Shih, R. Lo, S. Saati, R. Agrawal, M.S. Humayun, Y.-C. Tai, E. Meng, An electrochemical intraocular drug delivery device, Sens. Actuators A Phys. 143 (2008) 41–48.
[33] C. Neagu, H. Jansen, H. Gardeniers, M. Elwenspoek, The electrolysis of water: an actuation principle for MEMS with a big opportunity, Mechatronics 10 (2000) 571–581.
[34] J. Xie, Y. Miao, J. Shih, Q. He, J. Liu, Y.-C. Tai, T.D. Lee, An electrochemical pumping system for on-chip gradient generation, Anal. Chem. 76 (2004) 3756–3763.
[35] J.W. Munyan, H.V. Fuentes, M. Draper, R.T. Kelly, A.T. Woolley, Electrically actuated, pressure-driven microfluidic pumps, Lab Chip 3 (2003) 217–220.
[36] R.H. Liu, T. Nguyen, K. Schwarzkopf, H.S. Fuji, A. Petrova, T. Siuda, K. Peyvan, M. Bizak, D. Danley, A. McShea, Fully integrated miniature device for automated gene expression DNA microarray processing, Anal. Chem. 78 (2006) 1980–1986.
[37] S. Richter, N.-T. Nguyen, A. Wego, L. Pagel, Microfluidic devices on printed circuit board, in: F.E.H. Tay (Ed.), Microfluidics and BioMEMS Applications, Springer, New York, 2002, pp. 185–217.
[38] A. Wego, S. Richter, L. Pagel, Fluidic microsystems based on printed circuit board technology, J. Micromech. Microeng. 11 (2001) 528–531.
[39] R.H. Liu, J. Yang, R. Lenigk, J. Bonanno, P. Grodzinski, Self-contained, fully integrated biochip for sample preparation, polymerase chain reaction amplification, and DNA microarray detection, Anal. Chem. 76 (2004) 1824–1831.
[40] J. Guo, C.M. Li, Y. Kang, PDMS-film coated on PCB for AC impedance sensing of biological cells, Biomed. Microdevices 16 (2014) 681–686.
[41] D. Shi, J. Guo, L. Chen, C. Xia, Z. Yu, Y. Ai, C.M. Li, Y. Kang, Z. Wang, Differential microfluidic sensor on printed circuit board for biological cells analysis, Electrophoresis 36 (2015) 1854–1858.
[42] Y. Fu, Q. Yuan, J. Guo, Lab-on-PCB-based micro-cytometer for circulating tumor cells detection and enumeration, Microfluid. Nanofluid. 21 (2017) 20.
[43] P. Verma, D. Chatterjee, T. Nagarajan, Design and development of a modular valveless micropump on a printed circuit board for integrated electronic cooling, Proc. Inst. Mech. Eng. C 223 (2009) 953–963.
[44] N.-T. Nguyen, X. Huang, Miniature valveless pumps based on printed circuit board technique, Sens. Actuators A Phys. 88 (2001) 104–111.
[45] A. Wego, L. Pagel, A self-filling micropump based on PCB technology, Sens. Actuators A Phys. 88 (2001) 220–226.
[46] H. Vogt, R. Balzer, The bubble coverage of gas-evolving electrodes in stagnant electrolytes, Electrochim. Acta 50 (2005) 2073–2079.
[47] S.Z. Hua, F. Sachs, D.X. Yang, H.D. Chopra, Microfluidic actuation using electrochemically generated bubbles, Anal. Chem. 74 (2002) 6392–6396.
[48] N. Khosla, S. Venkatachalam, P. Somasundaran, Pulsed electrogeneration of bubbles for electroflotation, J. Appl. Electrochem. 21 (1991) 986–990.
[49] J. Xie, Integrated Parylene LC-ESI on a Chip, Ph.D. Dissertation, California Institute of Technology, 2005.
[50] R. Sheybani, E. Meng, High-efficiency MEMS electrochemical actuators and electrochemical impedance spectroscopy characterization, J. Microelectromech. Syst. 21 (2012) 1197–1208.
[51] M. Wang, Z. Wang, X. Gong, Z. Guo, The intensification technologies to water electrolysis for hydrogen production–a review, Renew. Sust. Energy Rev. 29 (2014) 573–588.
[52] S. Cherevko, A.A. Topalov, A.R. Zeradjanin, I. Katsounaros, K.J.J. Mayrhofer, Gold dissolution: towards understanding of noble metal corrosion, RSC Adv. 3 (2013) 16516–16527.
[53] A. Ursua, L.M. Gandia, P. Sanchis, Hydrogen production from water electrolysis: current status and future trends, Proc. IEEE 100 (2012) 410–426.
[54] K. Zeng, D. Zhang, Recent progress in alkaline water electrolysis for hydrogen production and applications, Prog. Energy Combust. Sci. 36 (2010) 307–326.
[55] R. De La Rica, C. Fernández-Sánchez, A. Baldi, Polysilicon interdigitated electrodes as impedimetric sensors, Electrochem. Commun. 8 (2006) 1239–1244.
[56] I. Uvarov, S. Lemekhov, A. Melenev, V. Naumov, O. Koroleva, M. Izyumov, V. Svetovoy, A simple electrochemical micropump: design and fabrication, J. Phys. Conf. Ser. 741 (2016) 012167.
[57] W.M. Haynes, CRC Handbook of Chemistry and Physics, 96th ed., CRC Press, Boca Raton, 2015.
[58] W. Olthuis, W. Streekstra, P. Bergveld, Theoretical and experimental determination of cell constants of planar-interdigitated electrolyte conductivity sensors, Sens. Actuators B Chem. 24 (1995) 252–256.
[59] Y. Temiz, A. Ferretti, Y. Leblebici, C. Guiducci, A comparative study on fabrication techniques for on-chip microelectrodes, Lab Chip 12 (2012) 4920–4928.
[60] C. Coombs, H. Holden, Printed Circuits Handbook, seventh ed., McGraw-Hill Education, New York, 2016.
[61] Y. Okinaka, Electrtoless Plating of Gold and Gold Alloys, Cambridge University Press, 1990.
[62] D.A. Ateya, A.A. Shah, S.Z. Hua, An electrolytically actuated micropump, Rev. Sci. Instrum. 75 (2004) 915–920.

[63] S. Yao, D.E. Hertzog, S. Zeng, J.C. Mikkelsen, J.G. Santiago, Porous glass electroosmotic pumps: design and experiments, J. Colloid Interface Sci. 268 (2003) 143–153.
[64] Y. Kim, J. Kim, K. Na, K. Rhee, Experimental and numerical studies on the performance of a polydimethylsiloxane valveless micropump, Proc. Inst. Mech. Eng. C 219 (2005) 1139–1145.
[65] L. Chen, S. Lee, J. Choo, E.K. Lee, Continuous dynamic flow micropumps for microfluid manipulation, J. Micromech. Microeng. 18 (2007) 013001.
[66] A. Olsson, G. Stemme, E. Stemme, A valve-less planar fluid pump with two pump chambers, Sens. Actuators A Phys. 47 (1995) 549–556.
[67] C.-H. Chen, J.G. Santiago, A planar electroosmotic micropump, J. Microelectromech. Syst. 11 (2002) 672–683.
[68] S. Zeng, C.-H. Chen, J.C. Mikkelsen, J.G. Santiago, Fabrication and characterization of electroosmotic micropumps, Sens. Actuators B Chem. 79 (2001) 107–114.
[69] L. Chen, H. Wang, J. Ma, C. Wang, Y. Guan, Fabrication and characterization of a multi-stage electroosmotic pump for liquid delivery, Sens. Actuators B Chem. 104 (2005) 117–123.
[70] R. Bodén, M. Lehto, U. Simu, G. Thornell, K. Hjort, J.-Å. Schweitz, A polymeric paraffin actuated high-pressure micropump, Sens. Actuators A Phys. 127 (2006) 88–93.

Biographies

Hakhyun Kim received a Master's degree in Department of Mechanical Engineering at Myongji University in 2018. He received his B.S. degree in Mechanical Engineering in 2016 from the same University. His research focused on microfluidics, electrochemistry and optimization of MEMS microfabrication processes. Now he works as a research engineer in a medical instrument company.

Heewon Hwang received a B.S. degree in the Department of Mechanical Engineering at Myongji University. Her research interest was opto-mechanical systems.

Seonhyeok Baek is an undergraduate student in the Department of Mechanical Engineering at Myongji University and expected to receive his B.S. degree in 2019. His research interest includes MEMS (Micro-Electro-Mechanical-Systems) and laser machining.

Dohyun Kim is an associate professor in the Department of Mechanical Engineering at Myongji University. He received a B.S. and M.S. degrees in Mechanical Engineering from Sogang University, Republic of Korea in 1993 and 2001 respectively. He received a Ph.D. degree in Electrical Engineering from University of California, Los Angeles, United States in 2008. Before starting his professorship at Myongji University, he worked as a postdoctoral scholar in the Bioengineering Department at University of California, Berkeley for 3 years. His research interest includes polymer microfabrication, microfluidic sensors and actuators, and microscale bioanalytical system for disease diagnostics.